NEUTRONS IN LIGHT NUCLEI AND NEUTRON TRANSFER IN REACTIONS WITH LIGHT NUCLEI

Naumenko M.A.[1,*], Samarin V.V.[1,2]

[1]Joint Institute for Nuclear Research, Dubna, Russian Federation
[2]Dubna State University, Dubna, Russian Federation
[*]E-mail: anaumenko@jinr.ru

Abstract. The energies and the probability densities for the ground states of ^{3,6}He nuclei have been calculated by Feynman's continual integrals method. The contribution of neutron transfer to experimental cross sections for formation of isotopes ^{44,46}Sc in reaction ^{3}He + ^{45}Sc, ^{46}Sc in reaction ^{6}He + ^{45}Sc, ^{65}Zn in reaction ^{6}He + ^{64}Zn, ^{196,198}Au in reactions ^{3,6}He + ^{197}Au has been evaluated. For this purpose, the time-dependent Schrödinger equation for the external neutrons of ^{3,6}He, ^{45}Sc and ^{197}Au nuclei has been solved. The contribution of fusion-evaporation is taken into account using the NRV evaporation code. Results of calculation are in satisfactory agreement with the experimental data.

Keywords: Nuclear structure; Few-body systems; Feynman's continual integrals; Clusters in light nuclei; Nuclear reactions; Neutron transfer; Time-dependent Schrödinger equation; Fusion-Evaporation.

Introduction

The properties of the ground states of light nuclei (e.g., ^{3,6}He) may be calculated by Feynman's continual integrals method in Euclidean time [1–3]. The few-body nucleus ^{3}He may be considered as consisting of two protons and a neutron, whereas the cluster nucleus ^{6}He may be considered as an α-cluster and two neutrons. Knowledge of the properties and the wave functions of the ground states of helium isotopes is necessary for the theoretical description of reactions involving them, and is also of interest from the point of view of studying the cluster structure and halos in light nuclei.

The processes of neutron transfer are widely studied both experimentally and theoretically. In this work, we show that in the low-energy reactions ^{3,6}He + ^{197}Au, ^{3,6}He + ^{45}Sc, ^{6}He + ^{64}Zn neutron transfer is one of the most important channels. These calculations are based on the numerical solution of the time-dependent Schrödinger equation (TDSE) [4, 5] for the external neutrons of ^{3,6}He, ^{45}Sc and ^{197}Au nuclei. Fusion-evaporation was taken into account using the statistical model code available in the NRV knowledge base [6]. Results of calculation demonstrate overall satisfactory agreement with the experimental data.

Ground states of ^{3,6}He nuclei

The details of Feynman's continual integrals method are given in Refs. [1–3]. The parallel Monte Carlo algorithm for numerical calculations within Feynman's continual integrals method in Euclidean time was developed and implemented in C++ programming language using NVIDIA CUDA technology [7]. The calculations were carried out on the heterogeneous cluster [8] of the Laboratory of Information Technologies, Joint Institute for Nuclear Research, Dubna.

The calculations were performed in the center of mass system using Jacobi coordinates. For a system of three particles, two of which have equal masses $m_1 = m_2 = m$ (two protons in ^{3}He or two neutrons in ^{6}He)

$$\mathbf{q} = \{\mathbf{x}, \mathbf{y}\},\ \mathbf{x} = \mathbf{r}_2 - \mathbf{r}_1,\ \mathbf{y} = \mathbf{r}_3 - \frac{1}{2}(\mathbf{r}_1 + \mathbf{r}_2). \quad (1)$$

Neutron-neutron, proton-proton and neutron-proton two-body strong interaction potentials $V_{i-j}(r)$ $(i, j = n, p)$ similar to the M3Y potential have been used

$$V_{i-j}(r) = \sum_{k=1}^{3} u_k \exp\left(-r^2/b_k^2\right). \quad (2)$$

The values of the parameters of these potentials are given in Ref. [3].

The probability density distribution $\Psi_0(x, y, \cos\theta)$ for the different configurations of the ^{3}He nucleus with the angle θ between the vectors $\mathbf{x}$ and $\mathbf{y}$ is shown in Fig. 1.

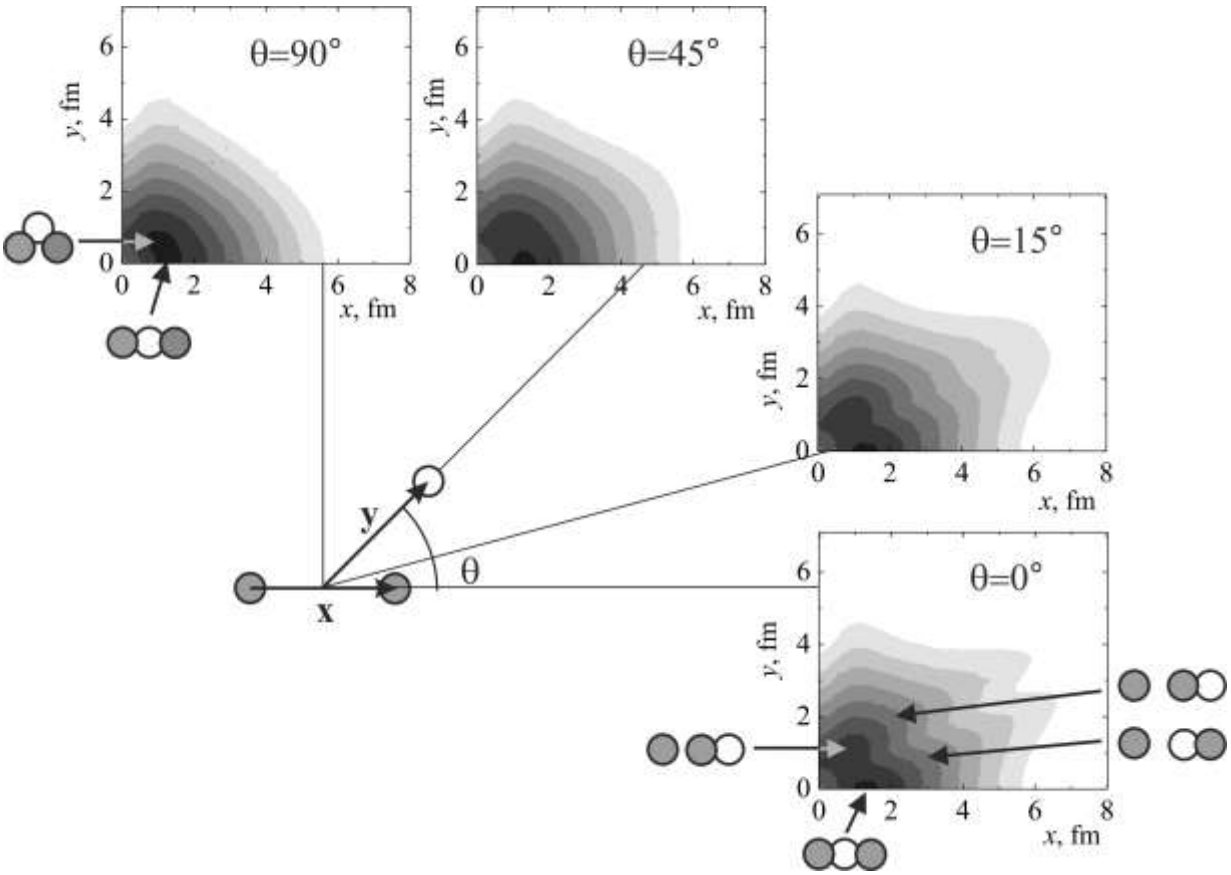

Fig. 1. The probability density $|\Psi_0|^2$ for the ^{3}He nucleus and the vectors in Jacobi coordinates; neutrons and protons are denoted as small empty circles and filled circles, respectively.

For the ^{3}He nucleus there are experimental data on the charge distribution [9]. The results of calculations of the charge distribution in the framework of the Feynman's continual integrals method for the ^{3}He nucleus in comparison with the experimental data [9] taken from the NRV knowledge base [6] are shown in Fig. 2. It can be seen that the calculations are in good agreement with the experimental data.

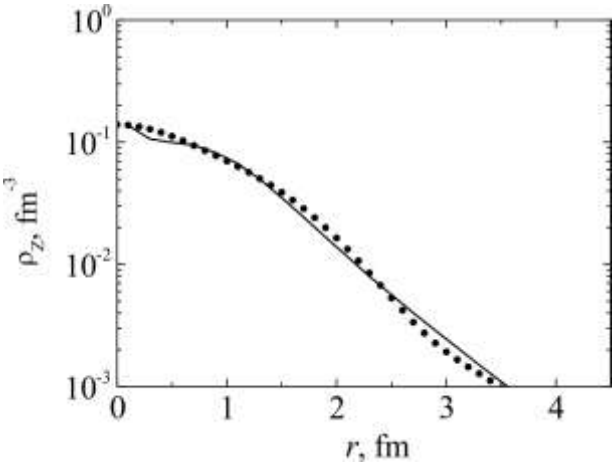

Fig. 2. A comparison of the theoretical charge distribution for the ^{3}He nucleus (solid line) with experimental data (circles) [9] taken from the NRV knowledge base [6].

Momentum distributions after breakup in nuclear reactions show that ^{6}He nucleus consists of an α-cluster core and a two-neutron cluster (e.g., [10]). The α-cluster-neutron interaction potential $V_{\alpha-n}(r)$ in the form of the combination of Woods-Saxon potentials was used

$$V_{\alpha-n}(r) = \sum_{i=1}^{s} U_i \left[1 + \exp\left((r - R_i)/a_i\right)\right]^{-1}, \qquad (3)$$

where $s = 2, 3$. The values of the parameters of these potentials are given in Ref. [3].

The probability density distribution $\Psi_0(x, y, \cos\theta)$ for the different configurations of the ^{6}He ($\alpha + n + n$) nucleus with the angle θ between the vectors $\mathbf{x}$ and $\mathbf{y}$ is shown in Fig. 3.

The obtained theoretical binding energies $E_B = -E_0$ are listed in Tab. 1 together with the experimental values taken from the NRV knowledge base [6]. For the ^{6}He nucleus the energy required for separation into an α-particle and two neutrons $E_S = -E_0$ is given. It is clear that the theoretical values are close enough to the experimental ones.

Table 1. Comparison of theoretical and experimental binding energies for the ground states of the studied few-body and α-cluster nuclei.

Atomic nucleus	Experimental value [6], MeV	Theoretical value, MeV
^{3}He	7.718	7.37 ± 0.3
^{6}He	0.97542	0.96 ± 0.05

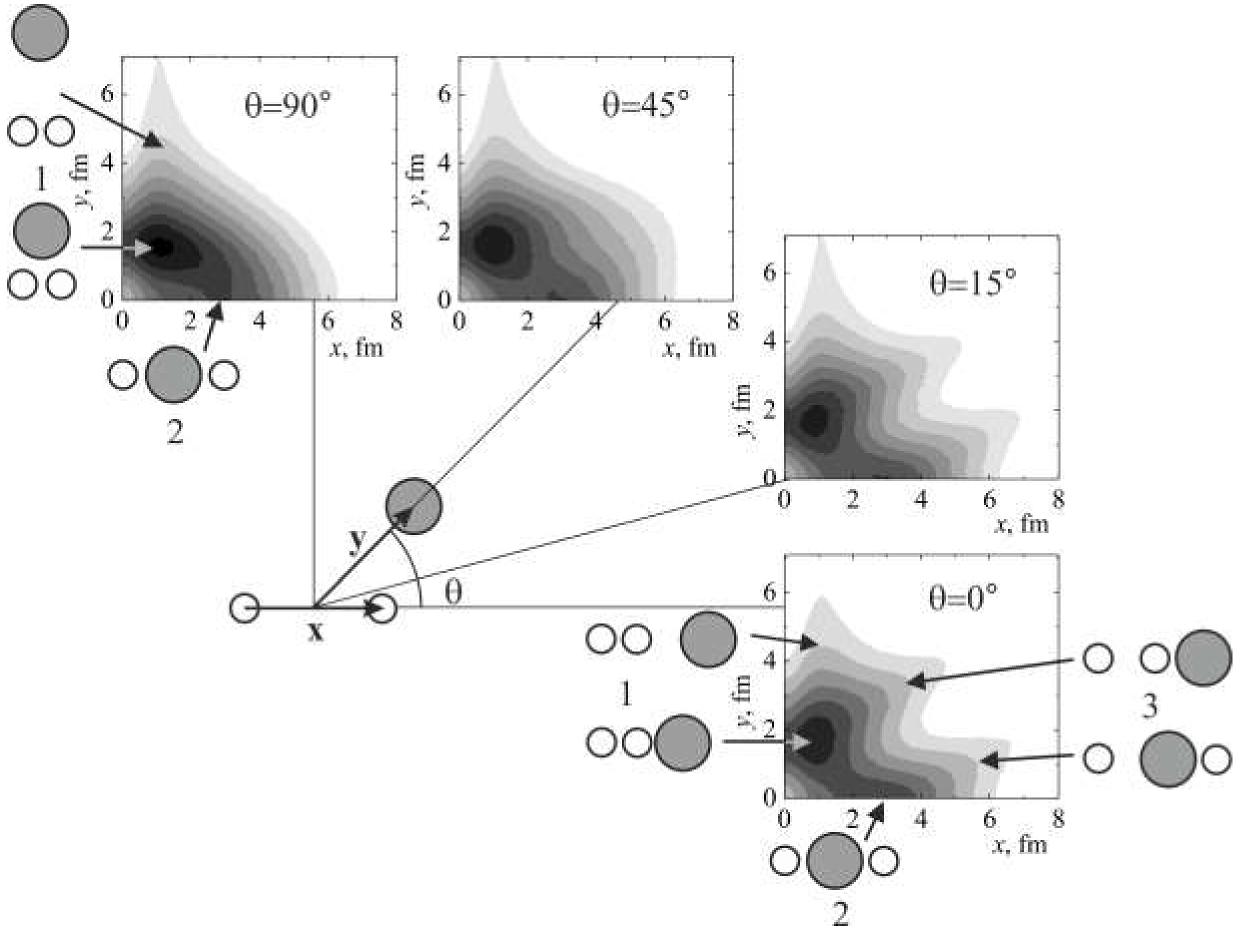

Fig. 3. The probability density $|\Psi_0|^2$ for the ^{6}He nucleus and the vectors in Jacobi coordinates; neutrons and α-clusters are denoted as small empty circles and large filled circles, respectively. The most probable configurations are α-cluster + dineutron (1) and the cigar configuration (2). The configuration n + ^{5}He (3) has low probability.

Time-dependent Schrödinger equation approach

For theoretical description of neutron transfer during collisions of heavy atomic nuclei we used the time-dependent Schrödinger equation (TDSE) approach [4, 5] for the external neutrons combined with the classical equations of motion of atomic nuclei

$$m_1\ddot{\vec{r}}_1 = -\nabla_{r_1} V_{12}(|\vec{r}_1 - \vec{r}_2|), \quad m_2\ddot{\vec{r}}_2 = -\nabla_{r_2} V_{12}(|\vec{r}_2 - \vec{r}_1|). \tag{4}$$

Here $\vec{r}_1(t)$, $\vec{r}_2(t)$ are the centers of nuclei with the masses m_1, m_2 and $V_{12}(r)$ is the potential energy of nuclear interaction. We may assume that before contact of the surfaces of spherical nuclei with the radii R_1, R_2 the potential energy of a neutron $W(\vec{r},t)$ is equal to the sum of its interaction energies with both nuclei.

The evolution of the components ψ_1, ψ_2 of the spinor wave function $\Psi(\vec{r},t)$ for the neutron with the mass m during the collision of nuclei was determined by Eq. (5) with the operator of the spin-orbit interaction $\hat{V}_{LS}(\vec{r},t)$

$$i\hbar\frac{\partial}{\partial t}\Psi(\vec{r},t) = \left\{-\frac{\hbar^2}{2m}\Delta + W(\vec{r},t) + \hat{V}_{LS}(\vec{r},t)\right\}\Psi(\vec{r},t). \tag{5}$$

The initial conditions for the wave functions were obtained using the shell model calculations with the parameters providing neutron separation energies close to the

experimental values. Based on the obtained results of Feynman's continual integrals method new parametrization of the mean field in the shell model for neutrons inside ^{3,6}He nuclei was proposed [1, 4].

The solution of the time-dependent Schrödinger equation provides the neutron transfer probability $p(b, E)$ [4, 5], where b is an impact parameter and E is the center-of-mass energy. The transfer cross section was calculated as an integral of $p(b, E)$ over the impact parameters of grazing collisions $b > b_{\min}$

$$\sigma(E) = \int_{b_{\min}}^{\infty} p(b,E)\, b db\,. \qquad (6)$$

In the analysis of experimental cross sections for formation of isotopes one must also take into account the possibility of their formation via fusion of colliding nuclei with the subsequent evaporation of nucleons and α-particles. For this purpose, we used computational code of the statistical model available in the NRV knowledge base [6].

Neutron transfer in reactions with ^{3,6}He

^{3}He + ^{45}Sc. Comparison of theoretical calculations with experimental cross sections for formation of isotopes ^{44}Sc and ^{46}Sc in reaction ^{3}He + ^{45}Sc is shown in Fig. 4*a* and Fig. 4*b*, respectively. Due to the low charge of the formed compound nucleus, the cross sections for the fusion with the subsequent evaporation of an α-particle and 2*p* are high enough and are respectively comparable with neutron pickup (^{44}Sc, Fig. 4*a*) and stripping (^{46}Sc, Fig. 4*b*) cross sections. The corresponding sums of neutron transfer and fusion-evaporation channels provide overall satisfactory agreement of calculation results with experimental data.

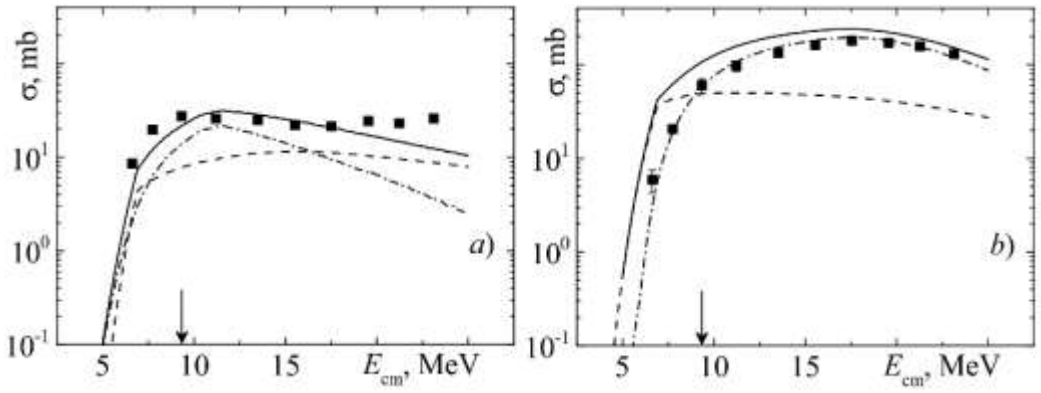

Fig. 4. The cross sections for formation of isotopes ^{44}Sc (*a*) and ^{46}Sc (*b*) in reaction ^{3}He + ^{45}Sc. Symbols are the experimental data from Refs. [11, 12], dash-dotted curves are the results of calculation of fusion-α-evaporation (*a*) and fusion-2*p*-evaporation (*b*) within the NRV knowledge base [6], dashed curves are the results neutron transfer calculations within the TDSE approach, solid curves are the sums of the corresponding transfer and fusion-evaporation channels. Here and below arrows indicate the position of the Coulomb barrier.

^{3}He + ^{197}Au. The experimental data on the formation of isotopes ^{196}Au and ^{198}Au in the reaction ^{3}He + ^{197}Au [13, 14] are compared to the theoretical calculations in Fig. 5*a* and Fig. 5*b*, respectively. The cross section for formation of the isotope ^{196}Au via fusion with the subsequent evaporation of an α-particle from the compound nucleus at energies above the Coulomb barrier is substantially (about two orders of magnitude) lower than the experimental data because the high Coulomb barrier prevents the emission of the α-particle from the compound nucleus with the high charge. Formation of ^{198}Au via fusion with the evaporation

of 2*p* from the compound nucleus was not observed in calculations. The calculated neutron pickup (^{196}Au, Fig. 5*a*) and stripping (^{198}Au, Fig. 5*b*) cross sections are in satisfactory agreement with the experimental data.

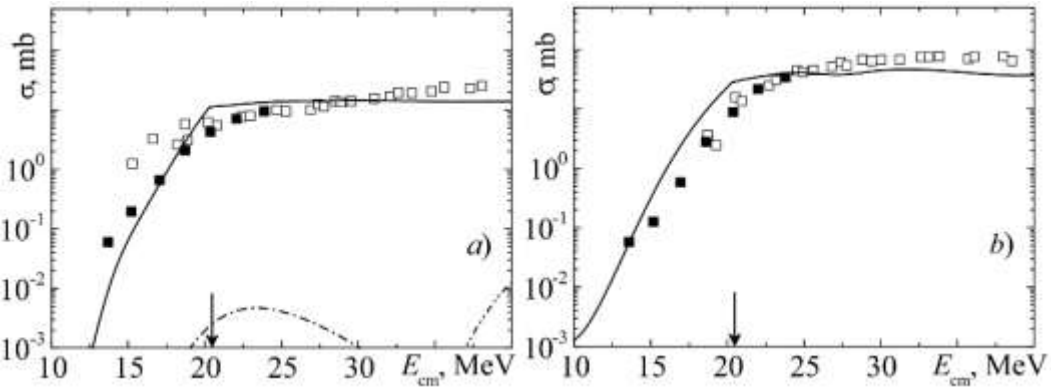

Fig. 5. The cross sections for formation of isotopes ^{196}Au (*a*) and ^{198}Au (*b*) in reaction ^{3}He + ^{197}Au. Symbols are the experimental data from Ref. [13] (filled squares) and Ref. [14] (empty squares), dash-dotted and dash-dot-dotted curves are respectively the results of calculation of fusion-α-evaporation and fusion-2*p*2*n*-evaporation within the NRV knowledge base [6], solid curves are the results neutron transfer calculations within the TDSE approach.

^{6}He + ^{45}Sc, ^{6}He + ^{64}Zn. Comparison of experimental data on the formation of isotopes ^{46}Sc in reaction ^{6}He + ^{45}Sc and ^{65}Zn in reaction ^{6}He + ^{64}Zn with the theoretical calculations is shown in Fig. 6*a* and Fig. 6*b*, respectively.

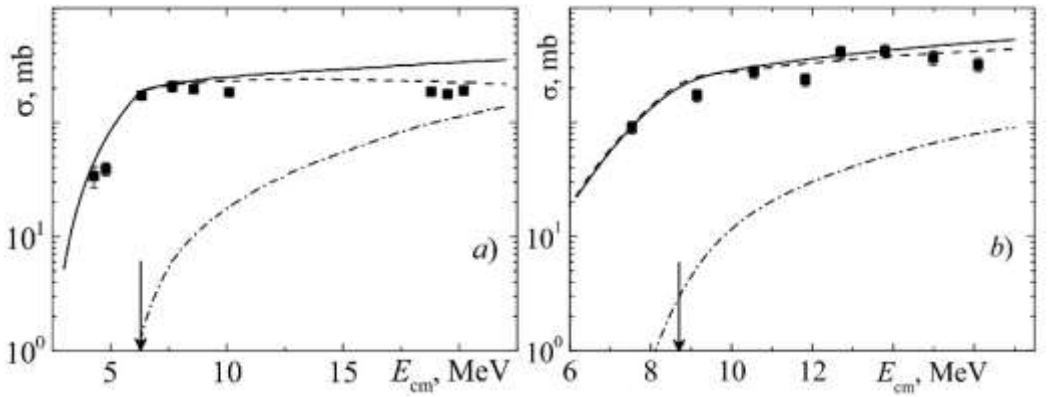

Fig. 6. The cross sections for formation of isotopes ^{46}Sc in reaction ^{6}He + ^{45}Sc (*a*) and ^{65}Zn in reaction ^{6}He + ^{64}Zn (*b*). Symbols are the experimental data from Ref. [15] (*a*) and Ref. [16] (*b*), dash-dotted curves are the results of calculation of fusion-α*n*-evaporation within the NRV knowledge base [6], dashed curves are the results neutron transfer calculations within the TDSE approach, solid curves are the sums of the corresponding transfer and fusion-evaporation channels.

The cross sections for the formation of the isotopes ^{46}Sc and ^{65}Zn via fusion with the subsequent evaporation of α*n* is significant at energies above the Coulomb barriers due to the low charge of the formed compound nucleus. In both cases, the corresponding sums of neutron transfer (stripping) and fusion-evaporation channels provide a satisfactory agreement between the calculated results and the experimental data.

^{6}He + ^{197}Au. Comparison of experimental data on the formation of isotopes ^{196}Au and ^{198}Au in the reaction ^{6}He + ^{197}Au with the theoretical calculations is shown in Fig. 7*a* and Fig. 7*b*, respectively. It can be seen that in this case the contribution of fusion with the subsequent evaporation to the experimental data is negligible due to the high Coulomb barrier of the formed compound nucleus preventing the evaporation of α-particles. It is an interesting fact that the experimental yield of the isotope ^{196}Au in the higher-energy region is comparable and even exceeds the yield of the isotope ^{198}Au.

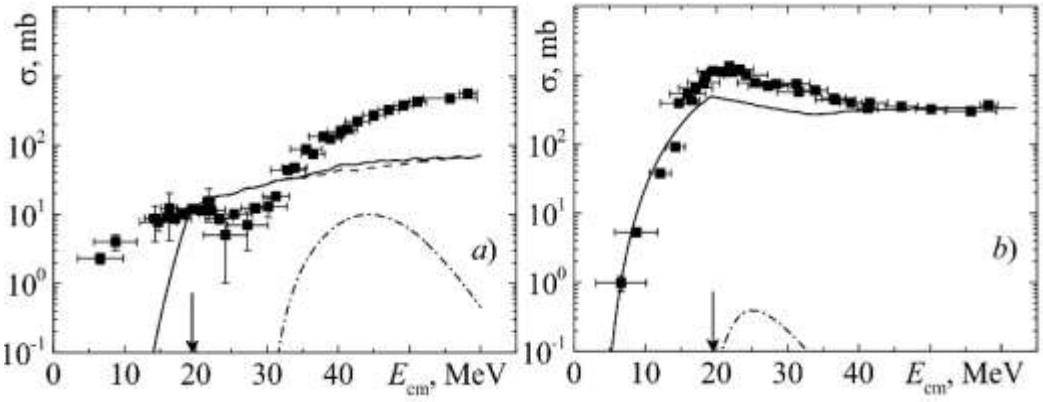

Fig. 7. The cross sections for formation of isotopes ^{196}Au (*a*) ^{198}Au (*b*) and in reaction ^{6}He + ^{197}Au. Symbols are the experimental data from Ref. [17], dash-dotted curves are the results of calculation of fusion-α3*n*-evaporation (*a*) and fusion-α*n*-evaporation (*b*) within the NRV knowledge base [6], dashed curves are the results neutron transfer calculations within the TDSE approach, solid curves are the sums of the corresponding transfer and fusion-evaporation channels.

Conclusions

The results of calculation within Feynman's continual integrals method in Euclidean time demonstrate that the theoretical values are close enough to the experimental ones for the studied nuclei. The obtained probability densities were used to propose new parametrization of mean field for neutrons inside ^{3,6}He nuclei within the shell model. The results of the shell model calculations served as the initial conditions in the time-dependent calculations of neutron transfer cross sections in reactions with the considered nuclei. The sums of neutron transfer and fusion-evaporation channels provided overall satisfactory agreement of calculation results with experimental data on formation of isotopes ^{44,46}Sc in reaction ^{3}He + ^{45}Sc, ^{46}Sc in reaction ^{6}He + ^{45}Sc, ^{65}Zn in reaction ^{6}He + ^{64}Zn, ^{196,198}Au in reactions ^{3,6}He + ^{197}Au. The statistical model calculations were performed using the computational code of the NRV knowledge base.

Acknowledgments

Authors thank Yu. E. Penionzhkevich, N. K. Skobelev, A. S. Denikin, and A. V. Karpov for fruitful discussions. The work was supported by Russian Science Foundation (RSF), grant No. 17-12-01170.

References

1. V. V. Samarin and M. A. Naumenko, Study of ground states of ^{3,4,6}He nuclides by Feynman's continual integrals method, *Bull. Russ. Acad. Sci.: Phys*. **80**, 283 (2016).

2. M. A. Naumenko, V. V. Samarin, Application of CUDA technology to calculation of ground states of few-body nuclei by Feynman's continual integrals method, *Supercomp. Front. Innov*. **3**, 80 (2016).
3. V. V. Samarin and M. A. Naumenko, Study of ground states of ^{3}H, ^{3,4,6}He, ^{6}Li, and ^{9}Be nuclei by Feynman's continual integrals method, *Phys. Atom. Nucl.* **80**, 877 (2017).
4. M. A. Naumenko, V. V. Samarin, Yu. E. Penionzhkevich, N. K. Skobelev, Near-barrier neutron transfer in reactions with ^{3}He nucleus, *Bull. Russ. Acad. Sci.: Phys.* **80**, 264 (2016).
5. M. A. Naumenko, V. V. Samarin, Yu. E. Penionzhkevich, N. K. Skobelev, Near-barrier neutron transfer in reactions ^{6}He + ^{45}Sc, ^{64}Zn, and ^{197}Au, *Bull. Russ. Acad. Sci.: Phys.* **81**, 710 (2017).
6. V. I. Zagrebaev, A. S. Denikin, A. V. Karpov, A. P. Alekseev, M. A. Naumenko, V. A. Rachkov, V. V. Samarin, V. V. Saiko, *NRV web knowledge base on low-energy nuclear physics.* URL: http://nrv.jinr.ru/.
7. NVIDIA CUDA. URL: http://developer.nvidia.com/cuda-zone/.
8. Heterogeneous cluster of LIT, JINR. URL: http://hybrilit.jinr.ru/.
9. G. A. Retzlaff, D. M. Skopik, ^{3}He charge form factors by nuclear recoil detection, *Phys. Rev.* C **29**, 1194 (1984).
10. Yu. E. Penionzhkevich, Reactions involving loosely bound cluster nuclei: heavy ions and new technologies, *Phys. Atom. Nucl*. **74**, 1615 (2011).
11. N. K. Skobelev, A. A. Kulko, Yu. E. Penionzhkevich *et al.*, Cross sections for production of ^{43}Sc, ^{44}Sc, and ^{46}Sc isotopes in the ^{45}Sc + ^{3}He reaction, *Phys. Part. Nucl. Lett.* **10**, 410 (2013).
12. N. K. Skobelev, A. A. Kulko, Yu. E. Penionzhkevich *et al.*, Cross sections of ^{43}Sc, ^{44}Sc, ^{46}Sc isotopes formed in the ^{45}Sc + ^{3}He reaction, *Bull. Russ. Acad. Sci.: Phys.* **77**, 795 (2013).
13. N. K. Skobelev, Yu. E. Penionzhkevich, E. I. Voskoboinik *et al.*, Fusion and transfer cross sections of ^{3}He induced reaction on Pt and Au in energy range 10-24.5 MeV, *Phys. Part. Nucl. Lett*. **11**, 114 (2014).
14. Y. Nagame, K. Sueki, S. Baba, and H. Nakahara, Isomeric yield in proton, ^{3}He, and α-particle induced reactions on ^{197}Au, *Phys. Rev. C* **41**, 889 (1990).
15. N. K. Skobelev, A. A. Kulko, V. Kroha *et al.,* Excitation functions for the radionuclide ^{46}Sc produced in the irradiation of ^{45}Sc with deuterons and ^{6}He, *J. Phys. G: Nucl. Part. Phys.* **38**, 035106 (2011).
16. V. Scuderi, A. Di Pietro, P. Figuera et al., Fusion and direct reactions for the system ^{6}He + ^{64}Zn at and below the Coulomb barrier, *Phys. Rev. C* **84**, 064604 (2011).
17. Yu. E. Penionzhkevich, R. A. Astabatyan , N. A. Demekhina *et al.,* Excitation functions of fusion reactions and neutron transfer in the interaction of ^{6}He with ^{197}Au and ^{206}Pb, *Eur. Phys. J. A* **31**, 185 (2007).